Chinese Journal of
POLYMER SCIENCE

RESEARCH ARTICLE

https://doi.org/10.1007/s10118-026-3846-8
Chinese J. Polym. Sci.

Dual-network Elastomer–Hydrogel Proton Exchange Membranes with Enhanced Conductivity and Mechanical Robustness

Ghasem Payam[a,b], Hamid Radmanesh[c*], and Kiyumars Jalili[a,b*]

[a] *Faculty of Polymer Engineering, Sahand University of Technology, New Town of Sahand, Tabriz 5331817634, Iran*
[b] *Institute of Polymeric Materials, Sahand University of Technology, New Town of Sahand, Tabriz 5331817634, Iran*
[c] *Faculty of Artificial Intelligence and Advanced Socinl Technologies, Islamic Azad University Central Tehran Branch, Tehran 1955847881, Iran*

Abstract The development of proton exchange membranes (PEMs) that simultaneously offer high proton conductivity and mechanical stability remains a critical challenge for fuel cell applications. Herein, we report a hybrid dual-network elastomer–hydrogel PEM (EH-PEM) synthesized *via in situ* polymerization of 2-acrylamido-2-methyl-1-propanesulfonic acid (AMPS), methyl methacrylate (MMA), and acrylic acid (AAc) within a hydrophilic methacrylated waterborne polyurethane (WPU–MA) elastomeric network. This design combines the elasticity and dimensional stability of WPU–MA with the hydrophilicity and ionic characteristics of the AMPS/AAc network, forming continuous pathways for efficient proton transport under hydrated conditions. The successful synthesis of WPU–MA was confirmed using Fourier-transform infrared spectroscopy (FTIR), dynamic light scattering (DLS), and gel permeation chromatography (GPC). The ion exchange capacity (IEC), water uptake, and electrochemical impedance spectroscopy (EIS) analyses further verified the formation of interconnected ionic domains. A series of membranes with varying AMPS contents were prepared, where increasing the AMPS content enhanced proton conductivity (16–98 mS·cm^{-1} at 80 °C) and reduced the activation energy for proton transport (9.6–9.7 kJ·mol^{-1}), while oxidative stability remained within 97%–62% retention after 96 h. Temperature-dependent conductivity and reduced activation energy suggest a combined Grotthuss–vehicle proton transport mechanism, where hydrogen bond rearrangements and sulfonic/carboxylic groups synergistically facilitated proton migration. This strategy provides a scalable platform for flexible hydrocarbon-based proton exchange membranes with markedly improved mechanical integrity compared to conventional AMPS-based hydrogel PEMs and demonstrates promising *ex situ* characteristics as a low-cost candidate material for potential use in proton exchange membrane fuel cells.

Keywords Proton exchange membrane; Elastomer–hydrogel; 2-Acrylamido-2-methyl-1-propanesulfonic acid (AMPS)–acrylic acid (AAc) copolymer; Waterborne polyurethane

Citation: Payam, G.; Radmanesh, H.; Jalili, K. Dual-network elastomer–hydrogel proton exchange membranes with enhanced conductivity and mechanical robustness. *Chinese J. Polym. Sci.* https://doi.org/10.1007/s10118-026-3846-8

INTRODUCTION

The growing global demand for sustainable and clean energy has intensified research into highly efficient energy conversion systems with minimal environmental impacts.[1–3] Among these technologies, proton exchange membrane fuel cells (PEMFCs) have attracted considerable attention because of their high energy density, rapid start-up capabilities, and relatively low operating temperatures.[4–8] The proton exchange membrane (PEM), the core component of PEMFCs, enables proton transport from the anode to the cathode, while preventing electron flow and fuel crossover.[9–11] Although Nafion, the most widely used commercial PEM, exhibits outstanding proton conductivity and chemical stability owing to its perfluorosulfonic acid backbone, its widespread commercialization is hindered by high production costs, degraded performance under low-humidity conditions, and high methanol permeability.[12–15] Consequently, the development of alternative hydrocarbon-based PEMs that offer high ionic conductivity, mechanical robustness, and low fuel crossover has become a primary focus of current research.[16]

Polymers containing sulfonic or carboxylic acid groups have been extensively explored as proton-conducting materials because of their strong acidity and high ion-exchange capacity.[17–20] Among them, 2-acrylamido-2-methyl-1-propanesulfonic acid (AMPS) has emerged as a promising candidate owing to its exceptional proton-donating ability, strong hydrophilicity, and thermal stability.[21,22] However, AMPS-based membranes frequently suffer from excessive water swelling and poor mechanical strength.[23,24] To address these limitations, various strategies, including copolymerization, crosslinking, and polymer blending, have been employed to balance ionic conductivity and mechanical integrity.[25,26] For instance, Diao *et al*.[19] reported crosslinked AMPS copolymers exhibiting a proton conductivity of 38 mS·cm^{-1} and significantly reduced methanol crossover. Similarly, Li *et al*.[22]

* Corresponding authors, E-mail: hamidradmanesh@iau.ac.ir (H.R.)
E-mail: k_jalili@sut.ac.ir (K.J.)
Received June 5, 2026; Accepted August 14, 2026; Published online November 10, 2026

© Chinese Chemical Society
Institute of Chemistry, Chinese Academy of Sciences

developed sulfonated poly(vinyl alcohol)/AMPS interpenetrating networks, achieving conductivities as high as 146 mS·cm^{-1} with excellent relative selectivity. Furthermore, Jiang *et al*.[17] fabricated a chitosan/P(AA-AMPS) membrane that demonstrated a conductivity of 36 mS·cm^{-1} and methanol permeability one order of magnitude lower than that of Nafion. These results show that the careful structural design of ionic polymers can significantly improve proton transport while maintaining mechanical stability, paving the way for the development of more efficient PEMs.

Flexible polymer backbones have been integrated into PEMs.[27] For instance, Hasani-Sadrabadi *et al*.[28] developed Nafion/AMPS-modified montmorillonite nanocomposites, which demonstrated remarkable improvements in tensile strength and elastic recovery owing to strong interfacial interactions between the polymer matrix and the inorganic phase. Similarly, Khalifa *et al*.[29] synthesized cellulose acetate grafted with AMPS and methyl methacrylate (MMA), achieving a proton conductivity of approximately 64 mS·cm^{-1} and an almost fourfold increase in Young's modulus compared to pristine cellulose membranes. In a related study, Kim *et al*.[25] showed that incorporating flexible phenyl-acrylate crosslinks within AMPS-based matrices significantly increased both the elongation at break and tensile resilience while maintaining high ionic conductivity. To address the trade-off between proton conduction and dimensional/mechanical stability in hydrated polymer electrolytes, various advanced structural modification strategies have recently been explored. For instance, incorporating inorganic nanostructures, such as natural clay frameworks or two-dimensional mica nanosheets, into polymer matrices provides robust physical reinforcement and tailored nanochannels that effectively retain protic species while maintaining structural integrity. Similarly, the design of ionogel-based systems and ionic liquid-embedded architectures has emerged as an effective approach for constructing continuous proton-conducting pathways with high chemical and thermal stabilities.[30–32]

A recent and promising strategy to enhance the mechanical properties of AMPS-based materials involves their incorporation into elastomer–hydrogel systems. Among the potential elastomeric components, waterborne polyurethane (WPU) stands out because of its highly favorable intrinsic properties. The methacrylated derivative, WPU–MA, can readily undergo radical copolymerization with vinyl monomers, enabling the formation of semi-interpenetrating or covalently cross-linked hybrid networks.[33,34] Building on these advancements, this study aims to design and synthesize hybrid elastomer–hydrogel PEMs (EH-PEM) *via in situ* free-radical copolymerization of AMPS, acrylic acid (AAc), and MMA, utilizing WPU–MA as an elastomeric crosslinker. Within this formulated system, each component serves a distinct, synergistic purpose: WPU–MA provides elasticity and structural stability under both hydration and thermal stress; AMPS supplies sulfonic acid groups to form continuous proton-conducting channels; AAc enhances water affinity and establishes hydrogen-bonding networks to facilitate proton mobility; MMA contributes to structural rigidity and hydrophobic balance to limit excessive swelling. This structural synergy yields a dual-phase elastomer–hydrogel architecture that successfully couples the high ionic conductivity of the hydrophilic domains with the mechanical toughness of the elastomeric segments.[35,36] This design strategy aims to achieve a proper balance between proton conductivity, mechanical durability, and thermal stability using a cost-effective and scalable process for next-generation polymer electrolyte membranes for fuel cell applications.

EXPERIMENTAL

Materials

Isophorone diisocyanate (IPDI, 99%), poly(ethylene glycol) (PEG, M_n=400 g·mol^{-1}), dimethylolpropionic acid (DMPA, 98%), triethylamine (TEA, 99%), ethylenediamine (EDA, 99%), hydroxyethyl methacrylate (HEMA, 97%), dibutyltin dilaurate (DBTDL, 95%), 2-acrylamido-2-methylpropanesulfonic acid (AMPS, 98%), methyl methacrylate (MMA, 99%), acrylic acid (AAc, 99%), azobisisobutyronitrile (AIBN, 98%), auxiliary chemicals, and solvents were purchased from Sigma–Aldrich and used without further purification. Deionized (DI) water was used for all experiments and formulations.

Membrane Preparation

Synthesis of waterborne polyurethane-methacrylate (WPU–MA)

WPU–MA was synthesized using a sequential five-step procedure, as illustrated in Fig. 1. Initially, PEG-400 (4000 mg, 10.0 mmol) and a drop of the DBTDL catalyst were charged into a three-necked flask equipped with a magnetic stirrer and a reflux condenser. The system was purged with nitrogen and heated to 60 °C. A solution of IPDI (6736 mg, 30.3 mmol) in 12 mL of dry acetone was then added, and the reaction proceeded under continuous stirring for 3 h to afford an NCO-terminated prepolymer. Following this, DMPA (1680 mg, 12.5 mmol) dissolved in DMF (3 mL) was added dropwise, and the mixture was maintained at 60 °C for an additional 2 h. The temperature was then lowered to 50 °C, and HEMA (650 mg, 5.0 mmol) in 3 mL of acetone was introduced to graft methacrylate functionalities onto the polyurethane chain ends, and the reaction mixture was stirred for 1 h. To neutralize the carboxyl groups from DMPA, TEA (1740 μL, 12.5 mmol) was added at 40 °C, followed by 30 min of stirring. Finally, chain extension and self-emulsification were achieved by dropwise addition of EDA (334 μL, 5.0 mmol) diluted in 12 mL of DI water at 30 °C, followed by vigorous mechanical stirring at 2000 r·min^{-1} for 1 h. Residual acetone was removed under reduced pressure, yielding a stable WPU–MA aqueous dispersion with a solid content of approximately 48 wt%.

Preparation of EH-PEM

EH-PEMs were prepared *via in situ* free-radical copolymerization using WPU–MA as an elastomeric crosslinker and AMPS, MMA, and AAc as co-monomers (Fig. 2). The precursor feed ratios and the corresponding sample designations are listed in Table 1. In a typical procedure, a predetermined amount of AMPS is dissolved in DMF at room temperature. Subsequently, WPU–MA, MMA, and AAc were added, and the mixture was stirred until a uniform solution was obtained. Polymerization was initiated by adding 100 μL of 10 wt% AIBN in DMF, followed by stirring for

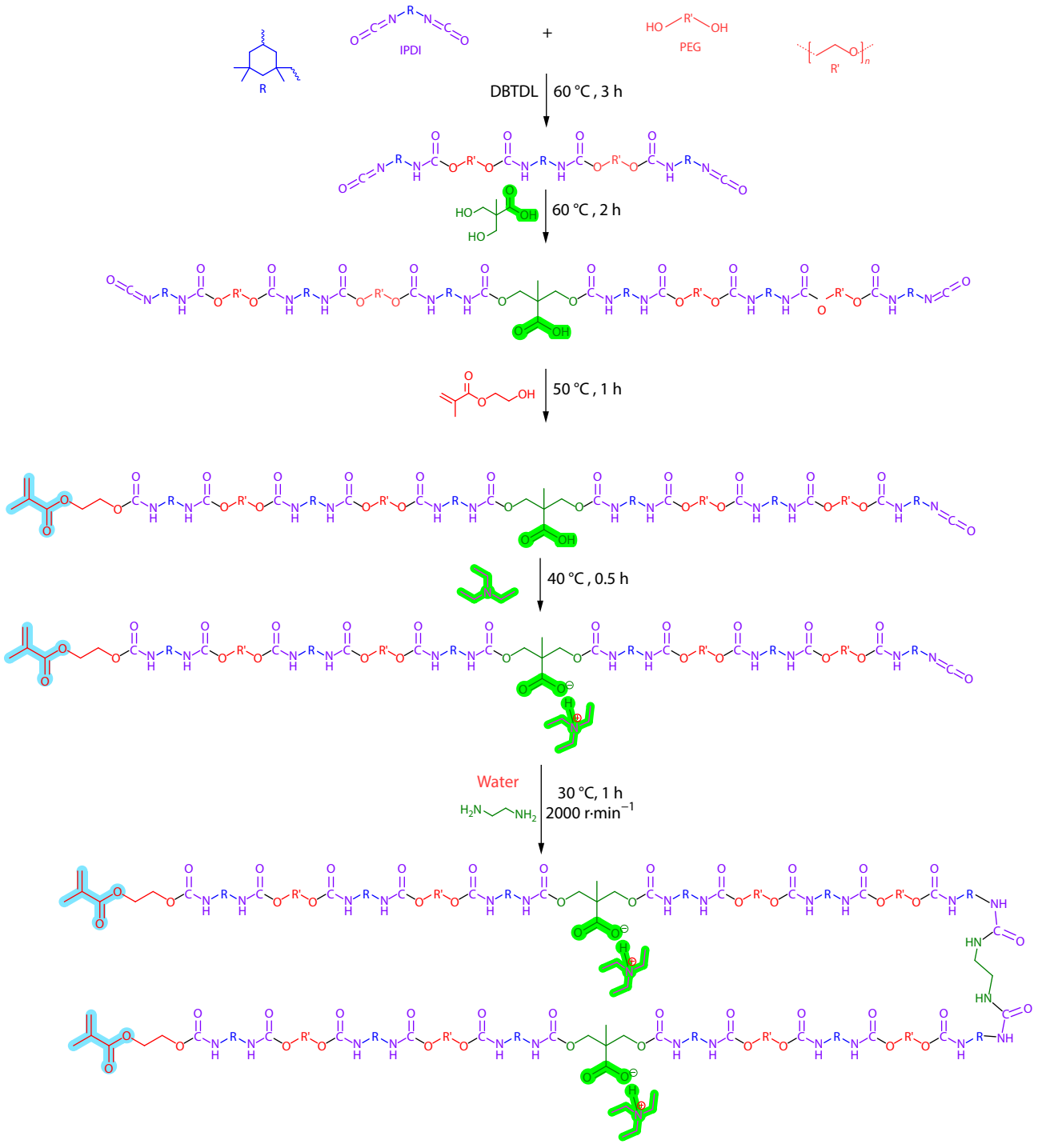


Fig. 1 Stepwise synthesis of WPU–MA, highlighting prepolymer formation, methacrylate functionalization, neutralization, and chain extension/self-emulsification.

10 min to ensure a uniform initiator distribution. The solution was then degassed under reduced pressure to eliminate the trapped air bubbles. The mixture was cast between two glass plates separated by a silicone spacer to control the membrane thickness, and cured in an oven at 60 °C for 24 h. After cooling to room temperature, the membranes were carefully demolded and immersed in 1 mol·L^{-1} HCl for 24 h to protonate the sulfonic and carboxylic acid groups and to remove any residual solvent. Finally, the films were washed and soaked in DI water for 24 h to remove trace HCl before characterization.

Characterization Methods

WPU–MA prepolymer characterization

Fourier transform infrared (FTIR) spectroscopy (Bruker Tensor 27) was employed to identify the functional groups of the synthesized WPU–MA, with spectra collected from 4000 cm^{-1} to

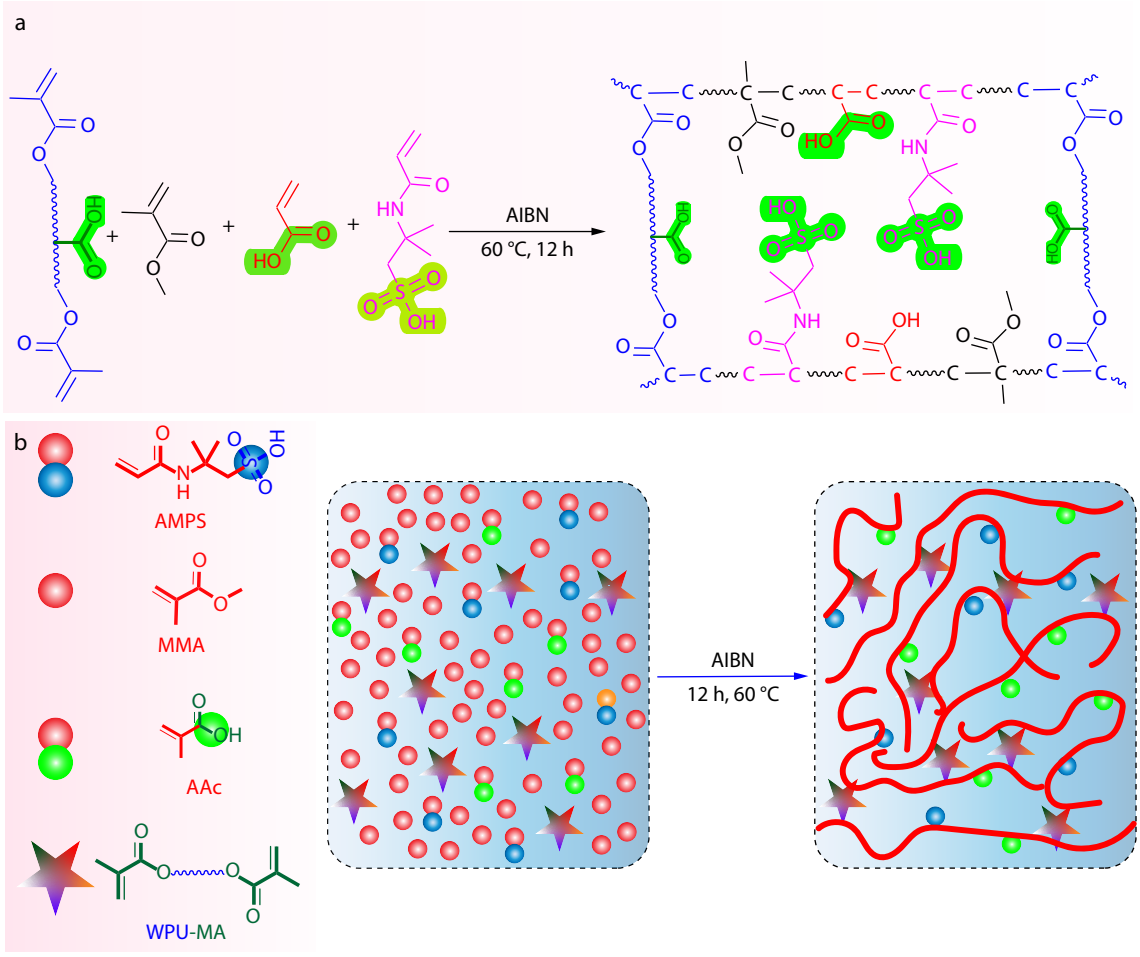


Fig. 2 Schematic illustration of EH–PEM preparation: (a) *in situ* copolymerization of WPU–MA with AMPS, MMA, and AAc, and (b) resulting membrane formation.

Table 1 Formulation of EH-PEM precursor mixtures with varying AMPS contents.

Sample	m_{WPU-MA} (mg)	m_{MMA} (mg)	m_{AMPS} (mg)	m_{AAc} (mg)	m_{AIBN} (mg)	m_{DMF} (mg)
A-00%	400	1200	0	600	10	1200
A-10%	400	1200	200	400	10	1200
A-20%	400	1200	400	200	10	1200
A-30%	400	1200	600	0	10	1200

400 cm^{-1}. Dynamic light scattering (DLS, Zetasizer Nano) was used to determine the hydrodynamic size and polydispersity index (PDI) at 25 °C, using diluted samples (about 0.1 $mg{\cdot}mL^{-1}$ in DI water). The molecular weight of WPU was measured by gel permeation chromatography (GPC) using THF as the eluent.

Field emission scanning electron microscopy (FESEM)

The morphological characteristics of the EH-PEM samples were examined by FESEM (VEGA, TESCAN, Czech Republic). The EH-PEM samples were freeze-dried and subsequently fractured to expose their cross sections for further analysis. Before the analysis, the samples were subjected to a gold-coating process to improve the imaging quality and ensure accurate observations.

Mechanical properties

The mechanical strengths of the membranes were evaluated using a universal testing machine (Zwick/Roell Z010). The specimens were shaped into dumbbells according to the ISO 527-2 Type B standard. Testing was conducted at room temperature at a crosshead speed of 10 $mm{\cdot}min^{-1}$.

Water uptake (WU)

The samples (1 cm × 1 cm) were dried in a vacuum oven at 40 °C for 24 h to obtain the dry mass (m_{dry}) and then soaked in deionized water at room temperature. After 48 h, excess surface water was gently removed using a filter paper before recording the wet mass (m_{wet}).

The WU was calculated using the following equation:

$$WU\,(\%) = \frac{m_{wet} - m_{dry}}{m_{dry}} \times 100 \quad (1)$$

Ion-exchange capacity (IEC)

The dried membrane samples were immersed in 1 $mol{\cdot}L^{-1}$ HCl for 24 h to completely protonate the —COOH and $-SO_3H$ groups. The membranes were then rinsed thoroughly with deionized water until a neutral pH was reached, and subse-

https://doi.org/10.1007/s10118-026-3846-8

quently placed in 1 mol·L^{-1} NaCl for 24 h to exchange H^+ with Na^+ ions. The released H^+ ions were titrated with 0.01 mol·L^{-1} NaOH using phenolphthalein as the indicator.

The IEC (mmol·g^{-1}) was calculated as:

$$\text{IEC} = \frac{V_{\text{NaOH}} \times c_{\text{NaOH}}}{m_{\text{dry}}} \quad (2)$$

where V_{NaOH} is the volume of the NaOH titrant (mL), c_{NaOH} is the molar concentration (mol·L^{-1}), and m_{dry} is the dry mass of the membrane (g). Each measurement was repeated thrice, and the average value was reported.

Proton conductivity measurement

The proton conductivity (σ) of the membranes was measured using electrochemical impedance spectroscopy (EIS) in a through-plane two-electrode configuration. Hydrated membrane discs (area≈0.63 cm^2) were placed between stainless steel electrodes and equilibrated in DI water for 24 h before testing. Impedance measurements were performed with an impedance analyzer over a frequency range of 0.2 MHz to 1 Hz by applying an AC amplitude of 10 mV at various temperatures. The resistance (R) was extracted from the high-frequency intercept of the Nyquist plots. The proton conductivity was calculated using the following equation:

$$\sigma = \frac{L}{R \times A} \quad (3)$$

where L is the membrane thickness (cm), R is the measured resistance (Ω), and A is the contact area (cm^2).

RESULTS AND DISCUSSION

Characterization of EH-PEM Membrane

Fig. 3(a) displays the FTIR spectra of the final WPU–MA product along with its precursors: the polyurethane-isocyanate prepolymer (PU-NCO), PEG, and HEMA. In the PEG spectrum, characteristic C—O stretching vibrations of the ether backbone appeared at 990–1210 cm^{-1}, whereas broad O—H stretching vibrations were observed between 3100 and 3600 cm^{-1}. The PU-NCO prepolymer spectrum showed a sharp absorption band corresponding to the —NCO group at 2100–2500 cm^{-1}. Furthermore, the HEMA spectrum featured characteristic bands for methacrylate groups (C=C and C=O) at 1600–1790 cm^{-1}. The WPU–MA spectrum confirms the successful synthesis by integrating key absorption bands from its precursors, including the N—H stretching of the urethane linkage (3200–3450 cm^{-1}),

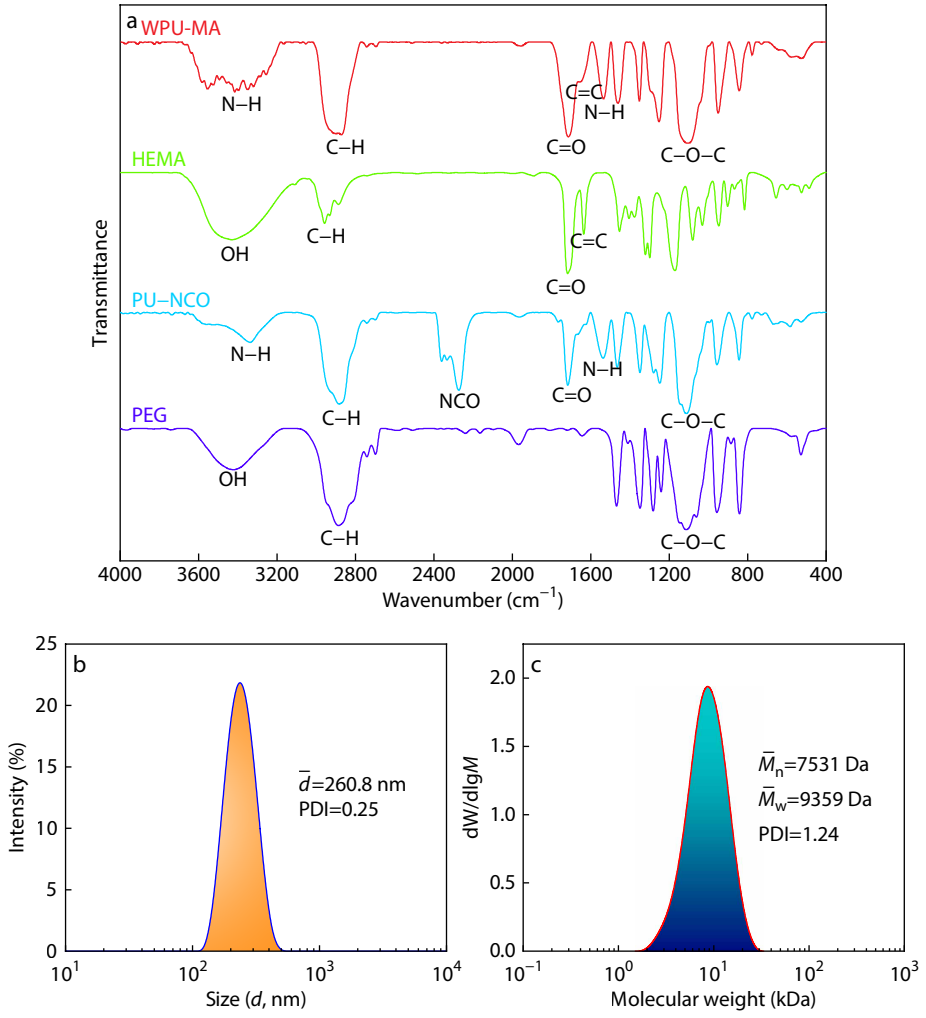


Fig. 3 Characterization of WPU–MA: (a) FTIR spectra of PEG, PU-NCO, HEMA, and WPU–MA product, (b) particle size distribution of the WPU–MA latex, and (c) molecular weight distribution of the polyurethane.

while showing the complete disappearance of the —NCO band. The particle size distribution of the WPU–MA aqueous dispersion was characterized by DLS, as shown in Fig. 3(b). The results revealed a narrow size distribution, with an average hydrodynamic diameter of approximately 261 nm and a low PDI of 0.25. The synthesized WPU–MA exhibited a number-average molecular weight (M_n) of 7531 Da and a weight-average molecular weight (M_w) of 9359 Da, according to GPC results (Fig. 3c). The resulting dispersity (PDI = M_w/M_n) of 1.24 indicates a well-controlled step-growth polymerization process.

Morphological Properties

Fig. 4 presents cross-sectional SEM micrographs of the EH-PEM membranes with varying AMPS content. As the AMPS content increased, a gradual evolution of the membrane morphology was observed, characterized by the formation of larger and more interconnected pores. This behavior is closely associated with the progressive substitution of AAc by AMPS in the precursor formulation. Because acrylic acid provides carboxylic acid groups capable of forming extensive intermolecular hydrogen bonds, replacing AAc with AMPS reduces the number of hydrogen-bonding sites within the polymer network. Consequently, the density of the physical crosslinking decreases, allowing greater polymer chain mobility during polymerization and solvent evaporation. The increased chain mobility facilitated the coalescence and growth of neighboring hydrophilic domains, resulting in a more open porous architecture with larger pore sizes. Furthermore, the higher concentration of sulfonic acid groups introduced by AMPS enhanced the hydrophilicity of the membrane, promoting greater water uptake and swelling of the ionic domains. These effects collectively contribute to the formation of more continuous proton-conducting pathways, which is consistent with the improved proton conductivity observed for membranes with higher AMPS content.

Physicochemical Properties of EH-PEM Membranes

The IEC of the EH-PEMs was measured to assess the density of the ionizable sites available for proton transport. As shown in Fig. 5(a), the IEC values progressively decreased from 3.9 mmol·g^{-1} for the A-00% sample to 1.3 mmol·g^{-1} for the A-30% sample. This decline reflects the reduced AAc content, as AAc, with a lower molecular weight, introduces more carboxylic acid (—COOH) groups per unit mass than the AMPS monomer. Consequently, substituting AAc with AMPS diminished the overall density of acidic functionalities. Nevertheless, this reduction in IEC does not translate into a decrease in proton conductivity. While there are fewer total acidic groups, the sulfonic acid ($-SO_3H$) groups provided by AMPS possess a significantly higher inherent acidity and degree of dissociation than the weaker —COOH groups. Therefore, the superior proton-donating capability of the $-SO_3H$ groups effectively compensated for the lower overall IEC, ensuring robust and enhanced proton conductivity. Furthermore, the theoretical IEC values estimated from the monomer feed ratios were higher than the experimental values. This discrepancy suggests partial neutralization of acidic groups during polymerization, alongside potential ion-pairing interactions between the —COOH/$-SO_3H$ groups and the cationic urethane residues within the WPU–MA matrix. Such interactions foster localized hydrogen-bonding networks that stabilize the membrane structure but concurrently reduce the effective number of exchangeable protons. As illustrated in Fig. 5(b), the WU of the EH-PEMs increased substantially with increasing AMPS content, rising from approximately 22% for A-00% to 262% for A-30%. This pronounced enhancement is primarily driven by the incorporation of the strongly hydrophilic $-SO_3H$ groups from AMPS, which effectively attracted and coordinated water molecules *via* ion-dipole interactions.

The oxidative stability of the EH-PEMs was evaluated by immersing the samples in 1 mol·L^{-1} H_2O_2 solution at room temperature for 48, 72, and 96 h (Figs. 5c and 5d). All membranes exhibited gradual mass loss over time owing to oxidative degradation initiated by hydroxyl (•OH) and hydroperoxyl (•OOH) radicals generated during the slow decomposition of hydrogen peroxide. The rate of degradation was highly dependent on the AMPS content. After 96 h, the A-00% membrane demonstrated the highest resistance, retaining about 97% of its initial mass, whereas the A-10%, A-20%, and A-30% samples retained approximately 77%, 69%, and 62%, respectively. This enhanced oxidative stability is primarily attributed to the absence of AMPS-derived sulfonic acid groups and the corresponding lower hydrophilicity and water uptake of A-00%, which reduce its susceptibility to oxidative degradation. For the AMPS-containing membranes, incorporation of the WPU–MA elastomeric segments still contributed to the overall durability relative to conventional hydrogel-based PEMs, as urethane linkages can partially quench radicals and dissipate local oxidative stress through dynamic hydrogen bonding and reversible network rearrangement, yielding a balanced performance for A-20% (retention of about 69% at 96 h).

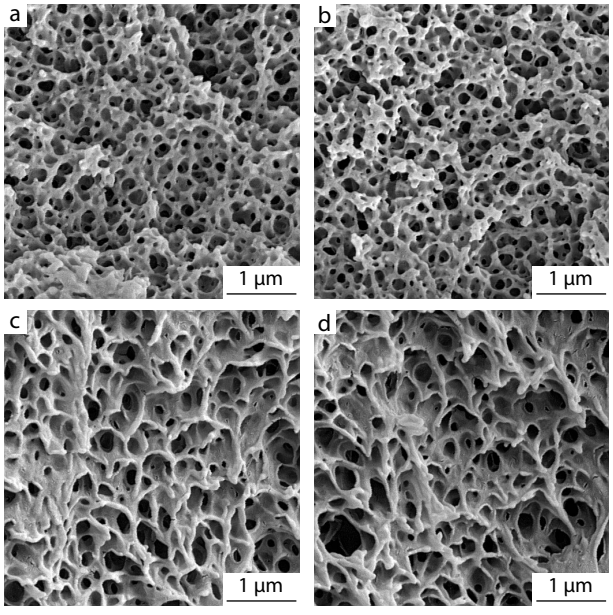


Fig. 4 Cross-sectional SEM images of EH-PEM membranes with different AMPS contents: (a) A-00%, (b) A-10%, (c) A-20%, and (d) A-30%.

Characterization of Mechanical Properties

The mechanical performance and deformation behavior of the prepared EH-PEMs were assessed through tensile testing (Fig. 6). The results indicate that the mechanical properties strongly depend on the monomer composition; increasing the AAc content significantly enhanced both the tensile strength and

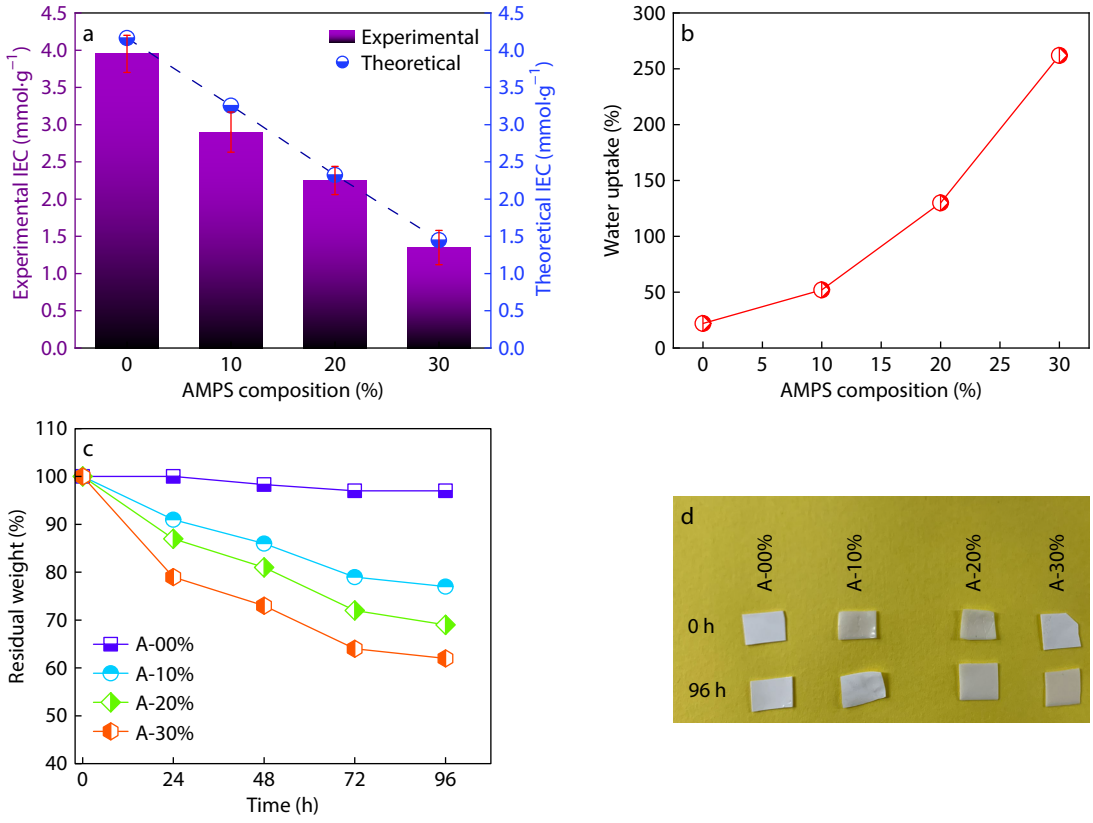


Fig. 5 Physicochemical properties of EH-PEMs: (a) ion-exchange capacity (IEC), (b) water uptake, and (c, d) oxidative stability in 1 mol·L^{-1} H_2O_2 at room temperature.

Young's modulus of the networks (Figs. 6a–6c). This behavior arises from the elevated IEC associated with higher AAc incorporation, which introduces a larger number of acidic functionalities compared to the equivalent mass fraction of AMPS. The increased density of carboxylic groups facilitated extensive hydrogen-bonding interactions, thereby reinforcing the physically crosslinked network. Such intensified intermolecular interactions account for the observed increase in the stiffness and strength, which is concomitant with a decline in the elongation at break. Furthermore, because all the specimens were evaluated under equilibrium swelling conditions, the absorbed water inevitably influenced their mechanical characteristics. Samples with higher AMPS fractions exhibited greater water uptake, wherein the absorbed water molecules effectively acted as plasticizers. This plasticization effect diminishes intermolecular chain interactions, consequently lowering the modulus and ultimate strength, while improving extensibility. Quantitatively, increasing the AMPS content decreased Young's modulus from 110 MPa to 10 MPa, increased the elongation at break from 100% to 260%, and reduced the ultimate tensile strength from 1.7 MPa to 0.9 MPa. The toughness initially increased from 1640 kJ·m^{-3} to 1760 kJ·m^{-3}, and then decreased to 1505 kJ·m^{-3}.

To evaluate the energy dissipation and fatigue resistance of the EH–PEMs, cyclic tensile loading–unloading tests were conducted for 10 consecutive cycles at a fixed strain. As shown in Figs. 6(d)–6(f), the A-20% sample demonstrated a significant self-recovery capability, retaining about 72% of its original form after the final cycle. However, increasing the AMPS content to 30% led to a drastic reduction in the recovery efficiency (dropping to about 15%), accompanied by a more pronounced residual strain. This disparity suggests that the A-20% composition maintains a more robust and reversible network of hydrogen bonds, which act as dynamic crosslinks to dissipate energy and facilitate elastic recovery. The inferior performance of A-30% may stem from an imbalance in the network density or increased chain slippage, which limits the reversible reformation of the hydrogen-bonded structure. Figs. 6(g)–6(i) further elucidate the structural and mechanical evolution of EH-PEMs. Fig. 6(g) shows the as-prepared sample immediately after demolding, which contained residual DMF and exhibited a soft, highly compliant nature. Upon solvent exchange with water (Fig. 6h), the sample underwent a distinct macroscopic transition from a flexible, soft state to a mechanically robust configuration, which is indicative of enhanced physical cross-linking and network densification. Fig. 6(i) shows the EH-PEMs under various deformation modes, including bending and twisting, underscoring their remarkable flexibility and resilience under mechanical stress.

Proton Conductivity and Electrochemical Behavior

EIS was conducted to investigate the bulk and interfacial resistances of the EH-PEMs. Figs. 7(a)–7(g) show the Nyquist plots for the samples with varying AMPS contents (A-00% to A-30%) recorded across a range of temperatures. All spectra exhibited a depressed semicircle in the high-frequency region, corresponding to bulk ionic conduction through the membrane, followed by an inclined linear tail at low frequencies, which arises from

https://doi.org/10.1007/s10118-026-3846-8

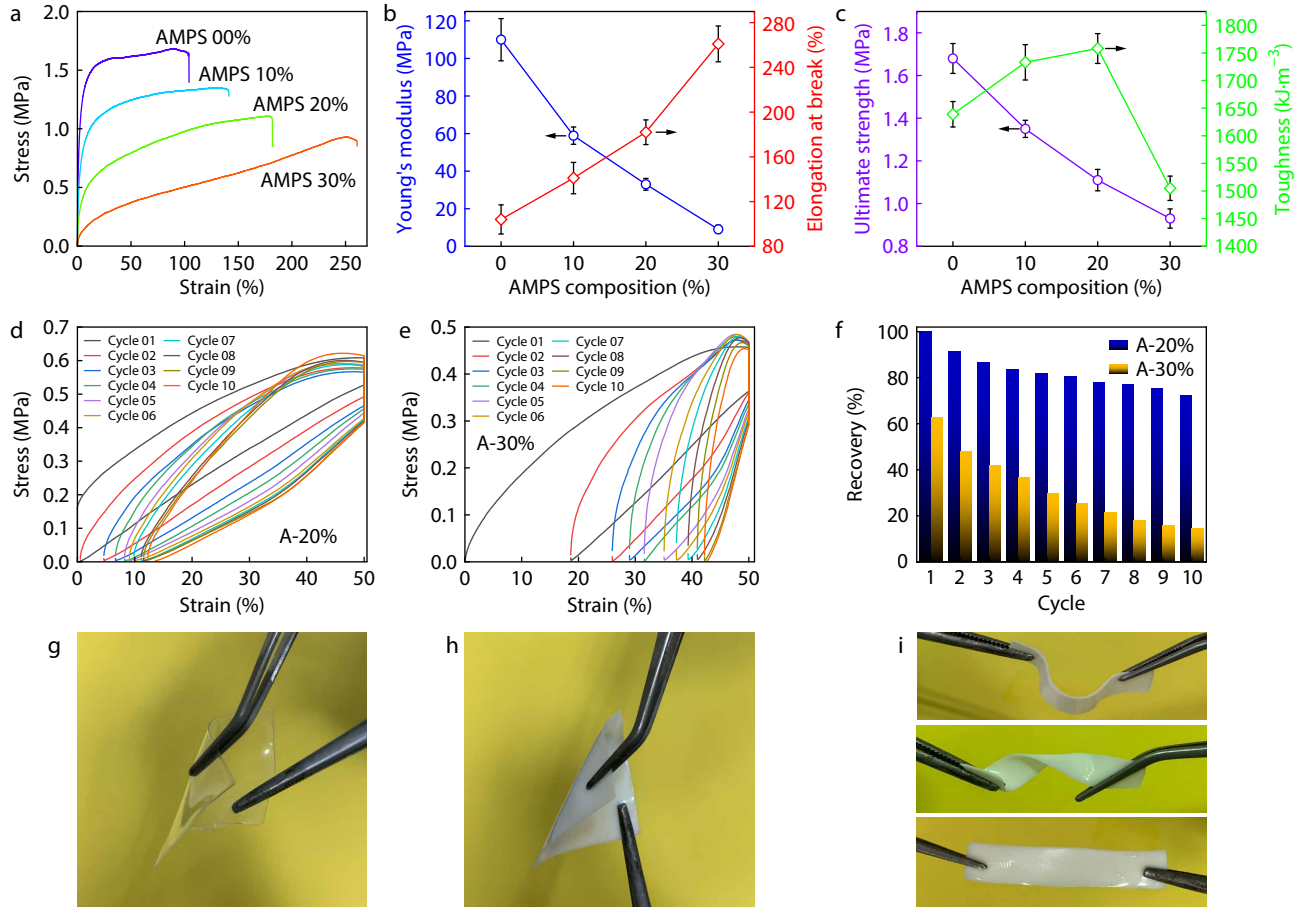


Fig. 6 Mechanical characterization of EH-PEMs. (a–c) Representative tensile stress-strain curves and the corresponding Young's modulus, elongation at break, ultimate tensile strength, and toughness of the EH-PEMs with varying AMPS contents; Fatigue resistance of (d) A-20% and (e) A-30% EH-PEM samples during 10 consecutive tensile loading–unloading cycles; (f) Recovery behavior of the EH-PEMs after cyclic tensile loading; (g) As-prepared sample immediately after demolding in the presence of DMF, showing a soft and compliant nature; (h) Sample after solvent exchange with water, exhibiting a transition to a stronger and more consolidated structure; (i) Optical images of the hydrogel under bending and twisting deformations, demonstrating excellent flexibility and mechanical durability.

electrode polarization and diffusion-related processes at the membrane–electrode interface. The deviation from an ideal semicircle suggests non-ideal capacitive behavior, likely due to structural heterogeneity and distributed relaxation times within the dual-network system. To quantitatively interpret the impedance response, the experimental data were fitted using the equivalent circuit model illustrated in Fig. 7(h), which consists of an interfacial resistance (R_{int}), a constant phase element (C_{int}) representing non-ideal capacitive behavior, and a Warburg diffusion element (W) associated with ion diffusion. With increasing temperature and AMPS content, the diameter of the impedance semicircle decreased markedly, indicating a significant reduction in membrane resistance and a corresponding increase in proton conductivity. This behavior can be explained by the presence of several synergistic factors. First, the incorporation of AMPS introduced a higher density of strongly acidic $-SO_3H$ groups, which exhibited greater dissociation than $-COOH$ groups, thereby increasing the concentration of mobile protons. Second, the formation of interconnected hydrophilic domains facilitates the development of continuous proton-conduction pathways. Third, elevated temperatures enhance the segmental mobility of polymer chains and promote water-assisted proton transport. Under fully hydrated conditions, these factors collectively favor a combined vehicular and Grotthuss-type proton transport mechanism, where proton hopping through hydrogen-bonded networks and the diffusion of hydronium ions occur simultaneously. As a result, membranes with a higher AMPS content exhibited markedly improved electrochemical performance, demonstrating the effectiveness of the dual-network design in optimizing proton transport.

The proton conductivities of the hybrid EH-PEMs (A-00% to A-30%) were evaluated using EIS over a temperature range of 20–80 °C under fully hydrated conditions. As depicted in the temperature conductivity profiles (Fig. 8a), the conductivity exhibited a consistent monotonic increase with temperature, highlighting the thermally activated nature of proton transport. Elevated temperatures enhance both the polymer segmental mobility and water self-diffusion, which facilitates the reorganization of hydrogen-bond networks and lowers the energy barrier for proton migration. Among the samples, the A-30% membrane exhibited the highest conductivity, reaching approximately 50–98 mS·cm^{-1} over the investigated temperature range, whereas the A-00% membrane, which lacks

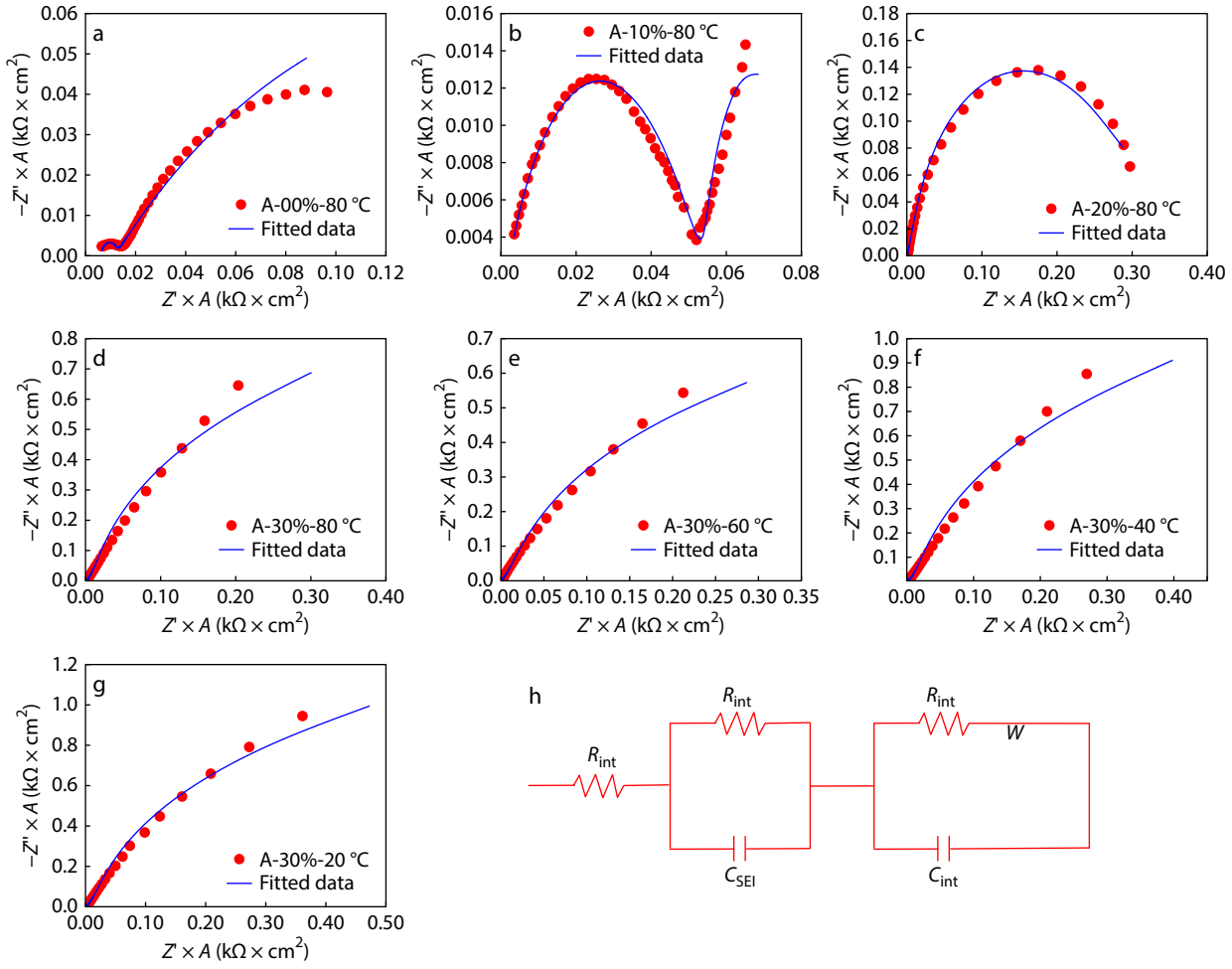


Fig. 7 (a–g) Nyquist plots of EH-PEMs with varying AMPS contents under different temperatures; (h) Along with the equivalent circuit model used for data fitting.

sulfonic acid groups, showed significantly lower values (about 3–16 mS·cm^{-1}). This pronounced difference highlights the critical role of AMPS-derived —SO_3H groups in generating efficient and continuous proton conduction pathways. Although the ion exchange capacity decreased with increasing AMPS content, the substantially higher proton conductivity suggests that proton transport was governed not only by the higher intrinsic acidity of the sulfonic acid groups, but also by the reorganization of the membrane morphology. Cross-sectional SEM observations revealed a finer and more homogeneous internal morphology at higher AMPS contents, which is consistent with the formation of more continuous hydrophilic pathways that facilitate through-plane proton transport.

Arrhenius plots of lnσ versus 1000/T (Fig. 8b) display nearly linear relationships, indicating that proton transport follows a thermally activated process. Calculated activation energies (E_a) decreased progressively with increasing AMPS content (Fig. 8c), suggesting that the incorporation of AMPS reduced the energetic barrier for proton migration through the formation of well-connected hydrophilic channels. The relatively low E_a of A-20% and A-30% (13.45 and 9.56 kJ·mol^{-1}) is consistent with the coexistence of Grotthuss (proton hopping) and vehicle (diffusion-assisted) proton transport mechanisms, as reported for similar proton exchange membranes in the literature.[16,17] This behavior is attributed to the formation of well-connected hydrophilic domains that promote proton hopping and facilitate long-range ion transport. In addition, the incorporation of the elastomeric WPU–MA backbone played a crucial role in maintaining mechanical integrity. This stabilization helps preserve the continuous ion-conduction pathways under operating conditions. The synergy between the elastic polyurethane domains and hydrophilic AMPS/AAc clusters effectively combined mechanical flexibility with high proton conductivity. This combination enables efficient proton transport while preserving the structural integrity, highlighting the potential of the WPU–MA/AMPS/AAc system for application in polymer electrolyte membranes for fuel cells.

A comparative analysis (Fig. 8d) revealed that the conductivity of the A-30% membrane was comparable to or exceeded that of several recently reported hydrogel-based and zwitterionic PEMs.[16,17,34] Additionally, the physicochemical and mechanical properties of Nafion 117, as the benchmark proton exchange membrane, together with those of the developed EH-PEM, are summarized in Table 2 to facilitate a direct comparison of their overall performance.

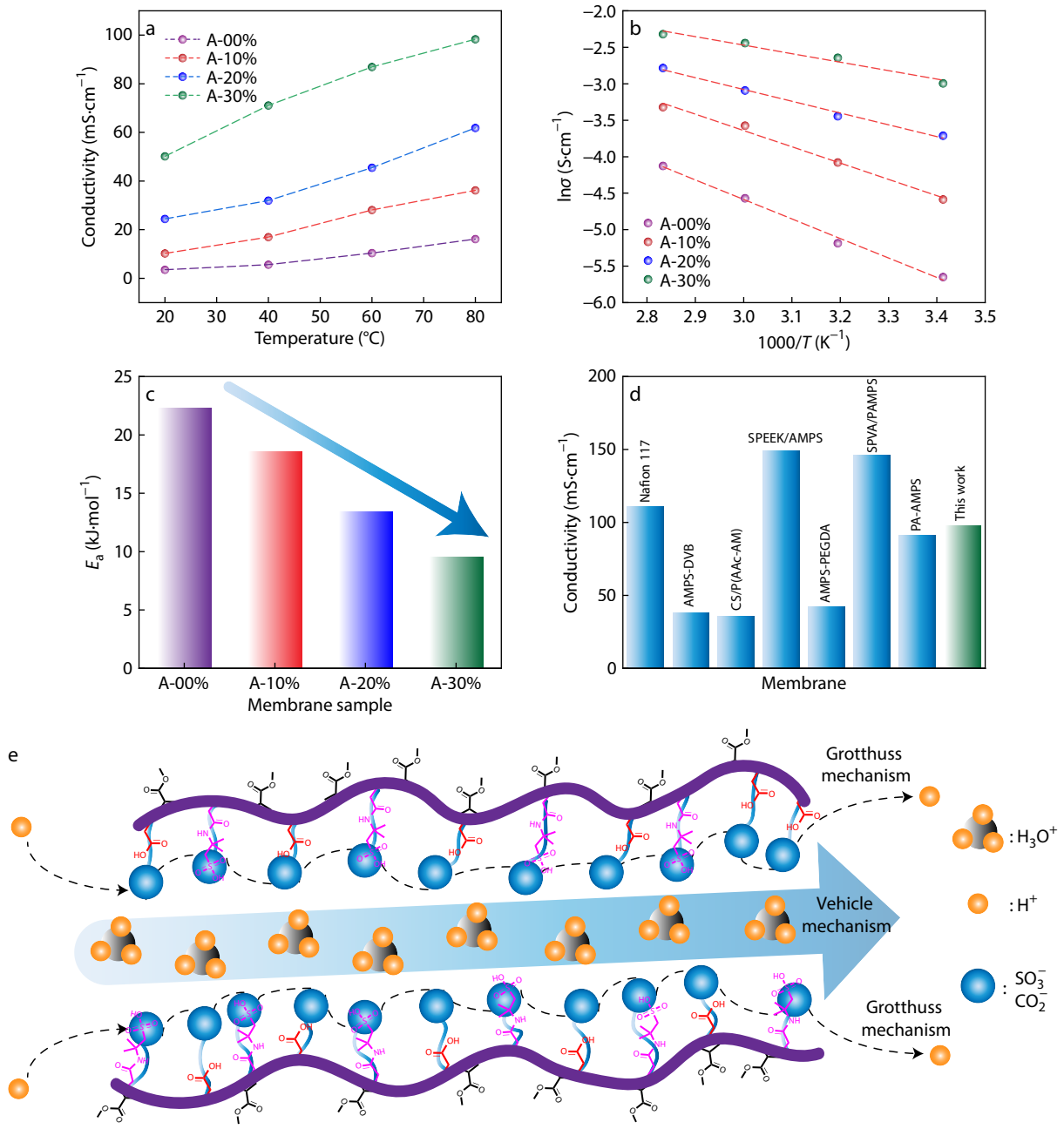


Fig. 8 (a) Temperature-dependent proton conductivity of A-00%–A-30% membranes; (b) Arrhenius plots of lnσ versus 1000/T with corresponding activation energies; (c) Variation of activation energy among the membranes; (d) Comparison of proton conductivity with reported PEMs; (e) Schematic illustration of proton transport mechanisms (Grotthuss and vehicular) within the membrane matrix.

Table 2 Comparison of the physicochemical properties of Nafion 117 and the developed EH-PEM membranes.

Membrane	Proton conductivity (mS·cm^{-1})	IEC (mmol·g^{-1})	Water uptake (%)	Tensile strength (MPa)	Young's modulus (MPa)
Nafion 117	5–83 (25–85 °C) [18] 69.6 (30 °C) [17] 59.8 [19] 81 [28] 78 [25, 37] 110 [16]	0.93 [38] 0.909 [17] 0.97 [19] 0.91 [4]	32–35 [39] 22–25 [40] 14.82 [19] 16 [4,37] 18.94 [41] 21 [4]	0.75–1 [38] 32–42 [39] 25.9–36.7 [42] 18.20 [41]	250–270 [42] 1 [25]
Our system	16–98 at 80 °C	1.35–3.95	22%–262%	0.9–1.7	10–110

https://doi.org/10.1007/s10118-026-3846-8

The schematic illustration in Fig. 8(e) further depicts the dual proton transport mechanism within the membrane matrix: (i) the Grotthuss mechanism, which involves proton hopping through hydrogen-bonded networks, and (ii) the vehicular mechanism, which is based on the diffusion of hydronium ions. The relatively low activation energy of the A-30% membrane (≈10 kJ·mol^{-1}) indicated the coexistence of these two mechanisms, with the Grotthuss pathway becoming increasingly dominant at higher AMPS contents because of the dense hydrogen-bonding network formed by $-SO_3H$ groups.[16]

CONCLUSIONS

Hybrid elastomer–hydrogel proton exchange membranes were successfully fabricated *via in situ* copolymerization of AMPS, AAc, and MMA using WPU–MA as an elastomeric crosslinking component. The resulting dual-network architecture integrated hydrophilic ionic domains with an elastic polyurethane framework, providing a balance between proton transport, mechanical integrity, and chemical stability. Increasing the AMPS content promoted the development of interconnected ionic domains and modified the hydrogen-bonding interactions within the network, contributing to enhanced proton transport pathways. Meanwhile, the WPU–MA segments provided structural support and maintained membrane flexibility under hydrated conditions. The optimized compositions (A-20% and A-30%) achieved proton conductivities of 62 and 98 mS·cm^{-1} at 80 °C, with activation energies of approximately 13.5 and 9.6 kJ·mol^{-1}, respectively. These activation energy values suggest that proton transport may involve contributions from both the Grotthuss-type and vehicle-assisted pathways, although further humidity-dependent measurements are required to quantitatively distinguish their relative contributions. The membranes also exhibited oxidative resistance in 1 mol·L^{-1} H_2O_2, retaining 69 and 62% of their initial mass after 96 h. The observed stability trend is associated with the combined effects of the ionic functionality, hydration level, and structural characteristics of the dual-network framework. The developed EH-PEMs represent a hydrocarbon-based polymer electrolyte platform with favorable *ex situ* proton transport and mechanical properties. This study establishes structure–property relationships within the elastomer–hydrogel dual-network system and provides a basis for further optimization of the membrane performance. Future work will focus on membrane–electrode assembly fabrication and single-cell PEMFC testing to evaluate the device-level performance. In addition, the effects of the WPU–MA content, crosslink-density regulation, reinforcement strategies, and systematic evaluation of whether the dynamic hydrogen-bonding network can impart self-healing capability will be investigated to further improve the membrane performance.

Conflict of Interests

The authors declare no interest conflict.

Data Availability Statement

The data supporting the findings of this study are available from the corresponding author upon reasonable request.

REFERENCES

1 Masson, V.; Lemonsu, A.; Hidalgo, J.; Voogt, J. Urban climates and climate change. *Annu. Rev. Environ. Resour.* **2020**, *45*, 411–444.
2 Adamantiades, A.; Kessides, I. Nuclear power for sustainable development: current status and future prospects. *Energy Policy* **2009**, *37*, 5149–5166.
3 Beswick, A. J.; Gibb, F. G. F.; Travis, K. P. Deep borehole disposal of nuclear waste: engineering challenges. *Proc. Inst. Civ. Eng. Energy* **2014**, *167*, 47–66.
4 Zuo, P.; Li, Y.; Wang, A.; Tan, R.; Liu, Y.; Liang, X.; Sheng, F.; Tang, G.; Ge, L.; Wu, L.; Song, Q.; McKeown, N. B.; Yang, Z.; Xu, T. Sulfonated microporous polymer membranes with fast and selective ion transport for electrochemical energy conversion and storage. *Angew. Chem. Int. Ed.* **2020**, *59*, 9564–9573.
5 Vinothkannan, M.; Hariprasad, R.; Ramakrishnan, S.; Kim, A. R.; Yoo, D. J. Potential bifunctional filler (CeO_2–ACNTs) for nafion matrix toward extended electrochemical power density and durability in proton-exchange membrane fuel cells operating at reduced relative humidity. *ACS Sustainable Chem. Eng.* **2019**, *7*, 12847–12857.
6 Staffell, I.; Scamman, D.; Velazquez Abad, A.; Balcombe, P.; Dodds, P. E.; Ekins, P.; Shah, N.; Ward, K. R. The role of hydrogen and fuel cells in the global energy system. *Energy Environ. Sci.* **2019**, *12*, 463–491.
7 Yang, F.; Xu, G.; Dou, Y.; Wang, B.; Zhang, H.; Wu, H.; Zhou, W.; Li, J. R.; Chen, B. A flexible metal–organic framework with a high density of sulfonic acid sites for proton conduction. *Nat. Energy* **2017**, *2*, 877–883.
8 Yang, Y.; He, X.; Zhang, P.; Andaloussi, Y. H.; Zhang, H.; Jiang, Z.; Chen, Y.; Ma, S.; Cheng, P.; Zhang, Z. Combined intrinsic and extrinsic proton conduction in robust covalent organic frameworks for hydrogen fuel cell applications. *Angew. Chem. Int. Ed.* **2020**, *59*, 3678–3684.
9 Thuc, V. D.; Kim, D. Ultra-thin, mechanically durable reinforced sulfonated poly(fluorenyl biphenyl) indole proton exchange membrane for fuel cell. *J. Membr. Sci.* **2024**, *694*, 122393.
10 Shen, X.; Liang, X.; Xu, Y.; Yu, W.; Li, Q.; Ge, X.; Wu, L.; Xu, T. *In-situ* growth of PPy/MnO_x radical quenching layer for durability enhancement of proton exchange membrane in PEMFCs. *J. Membr. Sci.* **2023**, *675*, 121556.
11 Li, Z.; Zhou, Y.; Hu, J.; Shi, C.; Liu, S.; Ge, Y.; Zhou, T.; Ye, Y. Incorporating flexible sulfonate-imidazolium ion pair-functionalized MOF in cross-linked polyvinyl alcohol membrane for achieving superprotonic conduction. *Chem. Eng. J.* **2024**, *480*, 148146.
12 Li, W.; Yang, F.; Lin, Z.; Sun, R.; Chen, L.; Xie, Y.; Pang, J.; Jiang, Z. Semi-crystalline sulfonated poly(ether ketone) proton exchange membranes: the trade-off of facile synthesis and performance. *J. Colloid Interface Sci.* **2023**, *645*, 493–501.
13 Liu, L.; Li, X.; Liu, Z.; Zhang, S.; Qian, L.; Chen, Z.; Li, J.; Fang, P.; He, C. High-performance fuel cells using Nafion composite membranes with alignment of sulfonated graphene oxides induced by a strong magnetic field. *J. Membr. Sci.* **2022**, *653*, 120516.
14 Yin, C.; Xiong, B.; Liu, Q.; Li, J.; Qian, L.; Zhou, Y.; He, C. Lateral-aligned sulfonated carbon-nanotubes/Nafion composite membranes with high proton conductivity and improved mechanical properties. *J. Membr. Sci.* **2019**, *591*, 117356.
15 Joseph, D.; Büsselmann, J.; Harms, C.; Henkensmeier, D.; Larsen, M. J.; Dyck, A.; Jang, J. H.; Kim, H.-J.; Nam, S. W. Porous nafion membranes. *J. Membr. Sci.* **2016**, *520*, 723–730.
16 Li, N.; Chen, J.; Li, J.; Xue, Y.; Li, Z.; Cai, L. Facile construction of polyacrylate membranes with pendent zwitterionic side-chains for high proton conduction. *Polymer* **2024**, *312*, 127681.

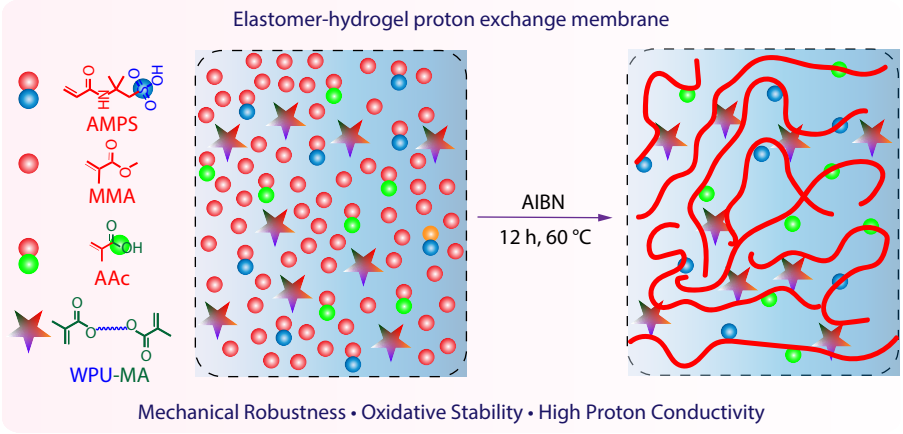
Graphical Abstract

Dual-network Elastomer–Hydrogel Proton Exchange Membranes with Enhanced Conductivity and Mechanical Robustness

Ghasem Payam, Hamid Radmanesh, and Kiyumars Jalili

Sahand University of Technology, Iran; Islamic Azad University Central Tehran Branch, Iran

An elastomer–hydrogel proton exchange membrane (EH-PEM) was developed by integrating waterborne polyurethanemethacrylate (WPU–MA) with acrylic ionic monomers through *in situ* polymerization. The dual-network architecture combined proton-conducting domains with a polyurethane framework, enabling enhanced proton conductivity and mechanical flexibility. The activation energy values suggest Grotthuss-type and vehicle-assisted proton transport pathways.



Chinese J. Polym. Sci. 2026 *https://doi.org/10.1007/s10118-026-3846-8*

17 Jiang, Z.; Zheng, X.; Wu, H.; Wang, J.; Wang, Y. Proton conducting CS/P(AA-AMPS) membrane with reduced methanol permeability for DMFCs. *J. Power Sources* **2008**, *180*, 143–153.
18 Zhong, S.; Cui, X.; Cai, H.; Fu, T.; Shao, K.; Na, H. Crosslinked SPEEK/AMPS blend membranes with high proton conductivity and low methanol diffusion coefficient for DMFC applications. *J. Power Sources* **2007**, *168*, 154–161.
19 Diao, H.; Yan, F.; Qiu, L.; Lu, J.; Lu, X.; Lin, B.; Li, Q.; Shang, S.; Liu, W.; Liu, J. High performance cross-linked poly(2-acrylamido-2-methylpropanesulfonic acid)-based proton exchange membranes for fuel cells. *Macromolecules* **2010**, *43*, 6398–6405.
20 Interial, L. G. D.; Benavides, R.; Morales-Acosta, D.; Francisco-Vieira, L.; Da Silva, L. Development of polymeric electrolytes for fuel cells: synthesis and characterization of new sulfonated polystyrene-co-acrylonitrile-co-butyl acrylate terpolymers. *Solid State Ion.* **2022**, *387*, 116066.
21 Manohar, M.; Kim, D. Synergistic effect of 2-acrylamido-2-methyl-1-propanesulfonic acid on the enhanced conductivity for fuel cell at low temperature. *Membranes* **2020**, *10*, 426.
22 Li, H. Q.; Liu, X. J.; Wang, H.; Yang, H.; Wang, Z.; He, J. Proton exchange membranes with cross-linked interpenetrating network of sulfonated polyvinyl alcohol and poly(2-acrylamido-2-methyl-1-propanesulfonic acid): excellent relative selectivity. *J. Membr. Sci.* **2020**, *595*, 117511.
23 Luo, G.; Jiang, J.; Wei, S.; Huang, C.; Chen, D.; Zhu, B.; Zhang, S. Introducing sulfonic acid polymers into MOF nanochannels for ultra-high Ba^{2+} adsorption capacity and proton conductivity. *Sep. Purif. Technol.* **2024**, *343*, 127133.
24 Rymsha, K. V.; Yu, Y. I.; Zhyhailo, M. M.; Demchyna, O. I.; Maksymych, V. M.; Ivashchyshyn, F. O. Hydrogels and their composites based on sulfo-containing acrylates: preparation, properties, and proton conductivity. *J. Solid State Electrochem.* **2024**, *28*, 555–563.
25 Kim, J. M.; Wang, Y.; Lin, Y.-H.; Yoon, J.; Huang, T.; Kim, D.-J.; Auad, M. L.; Beckingham, B. S. Fabrication and characterization of cross-linked phenyl-acrylate-based ion exchange membranes and performance in a direct urea fuel cell. *Ind. Eng. Chem. Res.* **2021**, *60*, 14856–14867.
26 Pal, S.; Mondal, R.; Chatterjee, U. Sulfonated polyvinylidene fluoride and functional copolymer based blend proton exchange membrane for fuel cell application and studies on methanol crossover. *Renew. Energy* **2021**, *170*, 974–984.
27 Che, Q.; Chen, N.; Yu, J.; Cheng, S. Sulfonated poly(ether ether) ketone/polyurethane composites doped with phosphoric acids for proton exchange membranes. *Solid State Ion.* **2016**, *289*, 199–206.
28 Hasani-Sadrabadi, M. M.; Dashtimoghadam, E.; Majedi, F. S.; Kabiri, K.; Solati-Hashjin, M.; Moaddel, H. Novel nanocomposite proton exchange membranes based on Nafion® and AMPS-modified montmorillonite for fuel cell applications. *J. Membr. Sci.* **2010**, *365*, 286–293.
29 Mesbah, F.; El Gayar, D.; Farag, H.; Tamer, T. M.; Omer, A. M.;

Mohy-Eldin, M. S.; Khalifa, R. E. Development of highly ionic conductive cellulose acetate-*g*-poly(2-acrylamido-2-methylpropane sulfonic acid-co-methyl methacrylate) graft copolymer membranes. *J. Saudi Chem. Soc.* **2021**, *25*, 101318.
30 Cai, D.; Zhou, Y.; Wang, B.; Ke, Y.; Xiao, B.; Hu, L.; Liu, Q.; Fu, X.; Li, X.; Geng, K.; Li, N. Mica ionogels-enhanced electrospun Nafion composite membranes: synergistic proton conduction and mechanical reinforcement for PEMFCs. *J. Membr. Sci.* **2025**, *732*, 124260.
31 Zhou, Y.; Wang, B.; Ling, Z.; Liu, Q.; Fu, X.; Zhang, Y.; Zhang, R.; Hu, S.; Zhao, F.; Li, X.; Bao, X.; Yang, J. Advances in ionogels for proton-exchange membranes. *Sci. Total Environ.* **2024**, *921*, 171099.
32 Liu, Q.; Wang, B.; Ling, Z.; Zhou, Y.; Hu, S.; Fu, X.; Zhang, R.; Zhang, Y.; Zhao, F.; Li, X.; Li, N.; Yang, J. Natural clay frameworks in membrane electrode assembly: challenges and perspectives. *Nano Energy* **2025**, *139*, 110980.
33 He, Y.; Ding, G.; Yu, R.; Yan, W.; Zhang, M.; Liu, R.; Jiang, L.; Wang, J.; Huang, W. A universal and simple method to obtain hydrogels with combined extreme mechanical properties and their application as tendon substitutes. *ACS Appl. Mater. Interfaces* **2022**, *14*, 54215−54224.
34 Xu, J.; Rong, X.; Chi, T.; Wang, M.; Wang, Y.; Yang, D.; Qiu, F. Preparation, characterization of UV-curable waterborne polyurethane-acrylate and the application in metal iron surface protection. *J. Appl. Polym. Sci.* **2013**, *130*, 3142−3152.
35 Yan, W.; He, Y.; Zhang, M.; Zhao, L.; Tian, F.; Hu, X.; Cheng, J.; Huang, W.; Ao, Y.; Yu, R. 3D printed elastomer-hydrogel composite meniscal scaffolds with biomimetic gradient structure and robust interface for preventing osteoarthritis and repairing meniscal injuries. *Adv. Funct. Mater.* **2024**, *34*, 2315580.
36 Payam, G.; Beighami, Z.; Jalili, K. Mimicking mechanical properties of human tissues with 3D printable polyurethane-based elastomeric-hydrogels. *Adv. Mater. New Coat.* **2022**, *11*, 3134−3142.
37 Kim, J. M.; Dobyns, B. M.; Zhao, R.; Beckingham, B. S. Multicomponent transport of methanol and acetate in a series of crosslinked PEGDA-AMPS cation exchange membranes. *J. Membr. Sci.* **2020**, *614*, 118486.
38 Sigwadi, R.; Dhlamini, M. S.; Mokrani, T.; Nemavhola, F.; Nonjola, P. F.; Msomi, P. F. The proton conductivity and mechanical properties of Nafion®/ZrP nanocomposite membrane. *Heliyon* **2019**, *5*, e02240.
39 Sahu, A. K.; Pitchumani, S.; Sridhar, P.; Shukla, A. K. Nafion and modified-Nafion membranes for polymer electrolyte fuel cells: an overview. *Bull. Mater. Sci.* **2009**, *32*, 285−294.
40 Walker, C. W. Jr. Proton-conducting polymer membrane comprised of a copolymer of 2-acrylamido-2-methylpropanesulfonic acid and 2-hydroxyethyl methacrylate. *J. Power Sources* **2002**, *110*, 144−151.
41 Abu-Saied, M. A.; Ali Soliman, E.; Abualnaj, K. M.; El Desouky, E. Highly conductive polyelectrolyte membranes poly(vinyl alcohol)/poly(2-acrylamido-2-methyl propane sulfonic acid) (PVA/PAMPs) for fuel cell application. *Polymers* **2021**, *13*, 2638.
42 Liu, D.; Kyriakides, S.; Case, S. W.; Lesko, J. J.; Li, Y.; McGrath, J. E. Tensile behavior of Nafion and sulfonated poly(arylene ether sulfone) copolymer membranes and its morphological correlations. *J. Polym. Sci., Part B: Polym. Phys.* **2006**, *44*, 1453−1465.

https://doi.org/10.1007/s10118-026-3846-8